Propulsion of bubble-based acoustic microswimmers

Nicolas Bertin[1],* Tamsin A. Spelman[2], Olivier Stephan[1], Laetitia Gredy[1], Michel Bouriau[1], Eric Lauga[2], and Philippe Marmottant[1]

[1] CNRS and University of Grenoble Alpes, Laboratoire Interdisciplinaire de Physique UMR 5588, B.P. 87, F-38402 St Martin d'Hères Cedex, France and

[2] Department of Applied Mathematics and Theoretical Physics, University of Cambridge, CB3 0WA, United Kingdom

Acoustic microswimmers present great potential for microfluidic applications and targeted drug delivery. Here we introduce armoured microbubbles (size range, $10 - 20\,\mu$m) made by three-dimensional microfabrication which allows the bubbles to last for hours even under forced oscillations. The acoustic resonance of the armoured microbubbles is found to be dictated by capillary forces and not by gas volume, and its measurements agree with a theoretical calculation. We further measure experimentally and predict theoretically the net propulsive flow generated by the bubble vibration. This flow, due to steady streaming in the fluid, can reach 100 mm/s, and is affected by the presence of nearby walls. Finally, microswimmers in motion are shown, either as spinning devices or free swimmers.

I. INTRODUCTION

Using microswimmers for transport and mixing purposes has been central to numerous research projects over the past decade [1–3]. Microswimmers act as propulsion devices that can carry a payload, and the propulsion jet can be used for mixing. Artificial microswimmers have recenlty been made possible because of two specific developments: on one side micro- and nano-fabrication [4, 5], and on the other contactless biocompatible devices such as magnetic fields [6–8], chemical engines [9, 10], or acoustically excited bubbles [5, 11–13], which are used to move objects at the microscopic scale.

One very promising actuation method exploits contactless acoustic sources. Sound waves can travel through biological tissues if their acoustic impedance is similar to the impedance of water so reflections are minimised [14]. A bubble subjected to ultrasound will pulsate intensely [15], especially when the driving frequency is near the resonance of the bubble. The pulsating bubble generates powerful acoustic streaming [16] that can be then be harnessed for propulsion. This mechanism has been used with some success at the $50 - 100\,\mu$m scale, in two-dimensional (2D) microchannels, with a contact disc transducer that has sharp resonance frequencies [5, 12, 13, 17].

In this paper, we demonstrate how to use three-dimensional (3D) microfabrication in order to build objects in the $10-20\,\mu$m range, that contain a microbubble − a device we call *armoured microbubble* (AMB). Unlike free air bubbles in water at room temperature [18], the AMBs are protected from dissolution, and have a long life even under acoustic forcing. We then show how to create a microswimmer by exciting an AMB with a contactless focused broadband transducer. Experiments and theory are used jointly to measure and predict resonance frequencies and strong streaming flows, with excellent agreement. We finally demonstrate how actuated AMBs may be used to induce swimming, in a manner which is affected by their environment and their shape.

II. FABRICATION, SETUP AND BUBBLE LIFESPAN

In order to fabricate 3D microobjects, we use a two-photon polymerisation setup (*TEEM Photonics*). The precision is on the order of the Nd:YAG microchip laser wavelength, 532 nm. The setup is mounted on the epifluorescence port of an inverted microscope. Fabrication pa-
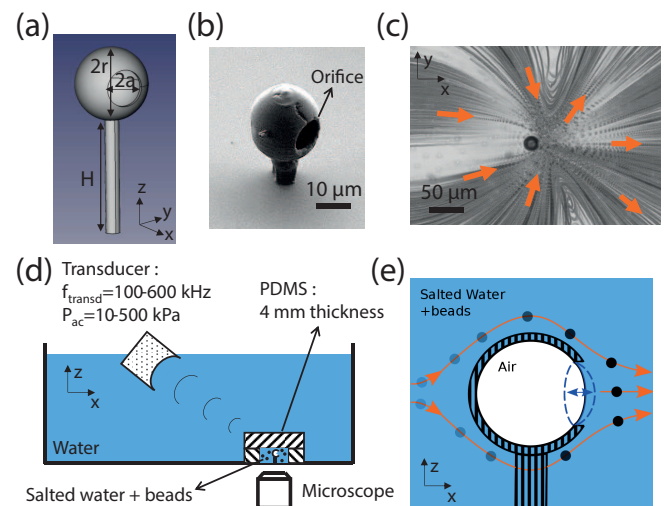

Figure 1: (a) *FreeCAD* design of a capsule with $r = 9\,\mu$m and $a = 5\,\mu$m on a pole of length $H = 30\,\mu$m; (b) SEM image of the device illustrated in (a); (c) Streamlines generated by device (b) submersed in water (viewed from below) at transducer's frequency $f_{transd} = 320$ kHz and acoustic pressure $P_{ac} = 9.2$ kPa; (d) Experimental setup; (e) Schematic of the bubble first vibration mode.

*Electronic address: nicolas.bertin@ujf-grenoble.fr

rameters are described in detail in Ref. [19]. The AMBs are designed on *FreeCAD* and fabricated on a glass coverslip (approx. 30 min per AMB) in the shape of a hollow capsule mounted on a pole (see Fig. 1a-b). The solid capsule is surrounded by liquid polymer which is ultimately washed away with acetone. The process generates $0.5\,\mu m$ thick shells, creating hollow objects that can be reinforced inside with plates or bars. The material used is ORMOCOMP©, which is biocompatible but not biodegradable. A crack at the top of the capsules is visible on scanning electron microscopy (SEM) images after fabrication (see Fig. 1b), but using a double shell design prevents leaks. To simulate an acoustic wave travelling through a microchannel, the coverslip is placed in a PDMS cell filled with 25 wt% NaCl water solution containing 2 µm spherical particles to observe the streamlines (see Fig. 1c-e). The cell is then placed inside a 1 L water tank (see Fig. 1d). Films are recorded with a *Phantom* v2511 high speed camera, with frame rates up to 10,000 frames per second, mounted on a IX73 *Olympus* microscope with x20 or x40 lenses. For sound emission, a contactless *Olympus* v381 transducer (500 kHz, focused, 330 kHz half-amplitude bandwidth) is used. Its broadbad emission will allow us to detect the true resonance of AMBs by scanning frequencies.

A challenging task when studying the acoustic streaming of AMBs is to prolong the life of the bubbles. Air in an AMB (see Fig. 1b) lasts for about 15 min in deionized water, and about 1 min when exposed to ultrasound. Condensation droplets appear inside the capsule, filling it gradually. We solved the problem by using a 25 wt% NaCl water solution, leading to an AMB lifetime of hours under ultrasound (a phosphate-buffered saline containing only a few percent of salt produces the same effect).

III. STREAMING

Having overcome the dissolution and lifetime challenge, we can now study the flow generated by AMBs for hours at a time. The vibration of the bubble interface under ultrasonic forcing results in a strong "acoustic streaming" jet [25]. Passive particles suspended in the fluid are seen flowing from the back and sides of fixed AMBs toward their opening before being pushed forwards away from the AMB (see Fig. 1c and 1e). The fluid jet directed away from the AMB provides the basis for a propulsion mechanism, and gives the order of magnitude of the velocity for a free swimming device.

We measured the maximum fluid velocity, v_{max}, of all the particles outside on the front side of the AMB. The particles trajectories are analysed with a predictive tracking algorithm [22]. A strong streaming flow is achieved with velocities up to 100 mm/s near the aperture (see Fig. 2a). For a $20\,\mu m$ AMB, this represents 5,000 body lengths per second, despite the PDMS cell which diminishes the acoustic pressure by 30% according to our measurements. This loss is higher than, for example, losses
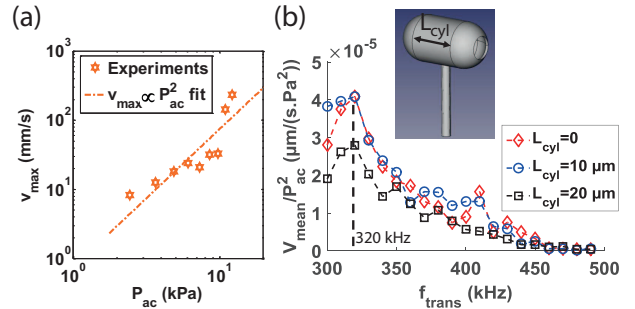

Figure 2: (a) Maximum flow velocity, v_{max}, as a function of the acoustic pressure, P_{ac}; (b) Normalised mean flow velocity, v_{mean}/P_{ac}^2, as a function of the transducer frequency, f_{trans}, for a voltage $U_{transd} = 7.6\,V_{pp}$ and three different values of L_{cyl}. The resonance frequency is measured to be 320 kHz.

due to ultrasound crossing organs (1 to 10% [14]). Moreover, the experimental points are in good agreement with a scaling $v_{max} \propto P_{ac}^2$, reflecting the quadratic nonlinearity of acoustic streaming.

IV. RESONANCE

In order to optimally control and actuate AMBs, we have to quantify and predict their first important characteristics, namely their resonance frequency. Free bubbles have well predicted resonances [15]. Recently, Wang et al [20] studied streaming from a 50 µm diameter bubble and noted that it generated a streaming flow of comparable velocities when excited in the range $1 - 100\,\mathrm{kHz}$. However, since they used a disc transducer with sharp resonances, they could not characterise the dependance of the the streaming velocity on the pressure amplitude.

In our case, the broadband transducer allows us to measure the resonance of the AMB. The mean velocity of the particles, v_{mean}, is measured in a $10 \times 100\,\mu m$ rectangle outside the opening, for three different AMBs with identical apertures but different volumes. Changing the volume is achieved by adding a cylindrical part of length L_{cyl} to the AMB (Fig. 2b). The case $L_{\mathrm{cyl}} = 0$ is the regular spherical AMB. A clear resonance is noted around $320\,\mathrm{kHz}$ for all shapes, with a 3 dB bandwith of approximately 30 kHz (see Fig. 2b). The resonance bandwidth means that a significant streaming ($v_{mean} \geq 100\,\mu m/s$) is generated for a large range of frequencies, which may be used for activating AMBs of different shapes with the same sound wave.

Can this measured resonance frequency of $320\,\mathrm{kHz}$ be rationalised? The origin of the resonance is related to that of a Helmoltz resonator, with the additional ingredient of the capillary restoring force. For a Helmoltz resonator the resonance is illustrated by a mass-spring system, with the mass that of the gas oscillating in the entrance and the elasticity due to the gas compressibility in the cavity. Here the mass is mainly given by the liq-

uid oscillating near the entrance, scaling like $m \sim \rho_l \pi a^2 l$, where ρ_l is the liquid density and l an effective length on the order of the entrance length. The elasticity is due to gas compressibility and additionally here to surface tension γ. Therefore two restoring forces act on the liquid mass, $F_{gas} = -k_{gas}(x - x_0)$ and $F_{cap} = -k_{cap}(x - x_0)$, with x the typical position of the apex of a surface deformation shown on Fig. 1e. The gas and capillary stiffness are respectively $k_{gas} \sim \kappa P(\pi a^2)^2/2V$ and $k_{cap} \sim 2\pi\gamma$ where V is the volume of gas in the capsule, P_0 is the atmospheric pressure, and $\kappa = 1.4$ is the adiabatic index. On the small scales relevant to our experiments, we obtain that the capillary stiffness is dominant and thus changing the AMB air volume V has less effect on the resonance frequency, $\omega_0 = ((k_{gas} + k_{cap})/m)^{1/2}$, than changing the aperture a. This is consistent with our findings in Fig. 2b.

In order to quantitatively predict the resonance frequency, we developed a fluid mechanics model incorporating the dominant capillary effects but neglecting the physics of the gas inside the bubble. Similarly to classical work on free bubbles, we describe the flow as irrotational (potential), but here we have mixed boundary conditions on the AMB surface assumed to be perfectly spherical: no normal velocity on the solid portion of the capsule and normal stress balanced by capillary stresses on the aperture gap. The model reduces to a generalised eigenvalue problem which can be solved numerically. In that case, the model predicts a resonance frequency $f_{th} = 333\,\text{kHz}$ for the first mode $n = 1$ of our AMB (using the measured value $\gamma = 69.7\,\text{mN/m}$ for 25 wt% salted water solution and particles). This is in excellent agreement with the experimental value of $320\,\text{kHz}$. The model can also be used to predict how the aperture size a affects the mode shapes in the limit $a \ll r$ and their resonance frequency. Specifically we predict the scaling

$$f_{th} \sim \left(\frac{n^3 \gamma}{\rho_l r^3 \theta_0^3} \right)^{1/2},$$

(1)

where $\theta_0 = \sin^{-1}(a/r)$ is the azimuthal angle where the aperture gap ends and n is the shape mode number.

The net flow created in the fluid as a result of the periodic oscillations of the free surface could be due to the combination of two phenomena, namely Eckart and steady streaming. Eckart streaming occurs when a sound wave dissipates part of its momentum in a viscous liquid, allowing that liquid to move [24]. Here the attenuation of waves occurs at much longer distances than the AMB size, so that we can discard the acoustic streaming that would follow the direction of propagation of the wave.

The second type of streaming, termed steady (or boundary acoustic) streaming, is then dominant [25]. It occurs in viscous boundary layers near walls (see [26]), for example at an air/water interface such as the surface of a bubble [27, 30]. There, momentum is imparted to the fluid resulting in a steady rectified fluid motion out of an oscillating forcing.
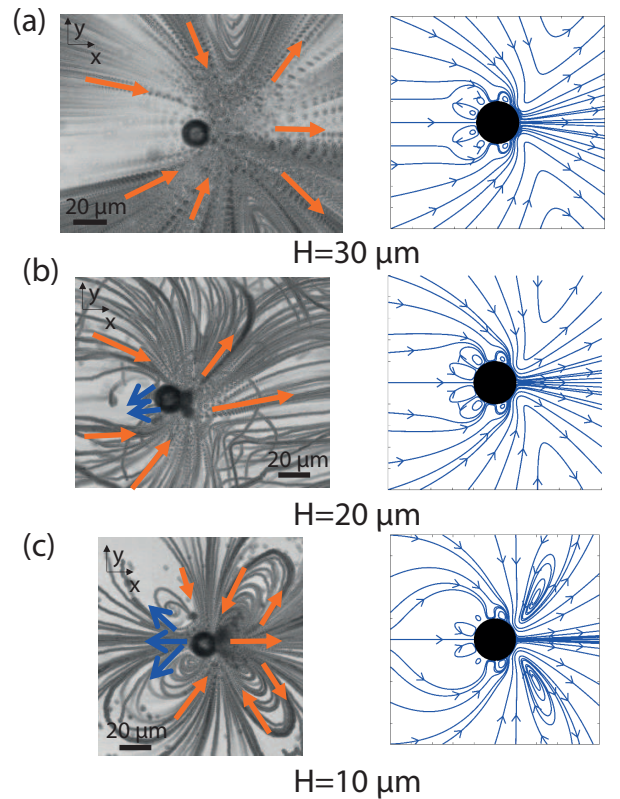

Figure 3: Streaming flows induced by AMBs (left) and theoretical streamline predictions (right) with different poles lengths H for $f_{transd} = 320\,\text{kHz}$ and $P_{ac} = 9.2\,\text{kPa}$.

V. MODEL

In order to predict the streaming flow, we developed a theoretical model. We assume the body is spherical and undergoes small-amplitude, axisymmetric surface shape oscillations [23]. Previous streaming work focused on simple shape oscillations of single material boundaries [28–31] and our model is able to generalise these results to a rigid capsule with an oscillating cap. We assume oscillations of small amplitude ϵr and small viscous boundary layer compared to the particle size (relative size δ), with $\epsilon \ll \delta \ll 1$. This is the relevant limit for micron-sized capsules in water being forced by ultrasound with kHz frequencies, and thus the relevant limit for our experiments.

In order to characterise the net streaming flow, we solve the problem as a power series expansion in the relative oscillation amplitude, ϵ. At $O(\epsilon)$ the equations have an analytical solution (this is an unsteady Stokes problem). At $O(\epsilon^2)$ we obtain the net streaming, which requires asymptotic matching to solve. The mixed boundary conditions of no motion on the rigid portion of the capsule and appropriate free-stress conditions on the aperture can then be applied to determine the surface shape oscillation, and hence the streaming this oscillation generates. The Lagrangian stream func-

tion in spherical coordinates (ρ, θ) around the AMB center is given by $\overline{\Psi}_L(\rho, \theta) = \sum_{n,m} A_{n,m} \rho^{-n} \int_{\cos \theta}^{1} P_m(x) \mathrm{d}x$, where $P_m(x)$ is the mth Legendre polynomial [23]. The coefficients $A_{n,m}$ are a sum of quadratic combinations of the amplitude of the vibration modes, described by a sum of spherical harmonics. As a result we obtain a streaming field that behaves at long distances from the AMB as a point-force flow (Stokeslet). The intensity of this Stokeslet, F_{thr}, provides the thrusting force on the microswimmer of order

$$F_{thr} \sim \epsilon^2 \rho_l r^4 f^2, \qquad (2)$$

with a prefactor which depends on the shape of the surface oscillation. For our AMB this prefactor is approximately 4, leading to the prediction $F_{thr} = 0.3 \, \mathrm{nN}$.

For an AMB away from the wall, the model accurately predicts the general shape of the streamlines using experimental parameters (see Fig. 3a). Beyond the current application, our model will also be relevant to any spherical oscillating body in this regime (e.g. spherical microorganisms) or other more complex spherical mechanical swimmers [5, 13, 23].

The 3D streaming flow generated by the devices may be affected by the proximity of solid boundaries. A transport AMB would travel in tight channels (e.g. biological) and it is important to understand how the propulsion may be affected by the walls. To that purpose, we fabricated AMBs with different poles lengths, H, and compared the shapes of the streamlines. The effect of the value of H is noticeable (see Fig. 3a-c): at large distances from the wall the fluid is pushed forward ($+x$ direction) everywhere, while close to the wall, a (small) backward flow appears behind the capsule ($-x$ direction). Closed circulation regions in the flow also appear near surfaces. We thus conjecture that propulsion may decrease in efficiency due to the backward flow occurring when AMBs approach boundaries.

The presence of a boundary was incorporated in the analytic streaming model by adding the image system for the leading-order Stokeslet flow decaying as $1/r$ [33] and next order Stresslet decaying as $1/r^2$ [34]. Our model predicts the increasing efficiency of the propulsion away from the wall. Indeed, recirculation patterns in front of the AMB are closed for $H = 10 \, \mu m$ and open up for $H = 20$ and $30 \, \mu m$. The general flow pattern is also well predicted by the model. The model is not able to predict the small backward flow seen experimentally, and a full numerical approach would be required to capture all near-field features.

VI. SWIMMERS

With our understanding of the physics of force generation, we can now use these forces to generate propulsion. As AMBs tend to stick to the substrate after fabrication, we use a tungstene probe mounted on a microstage
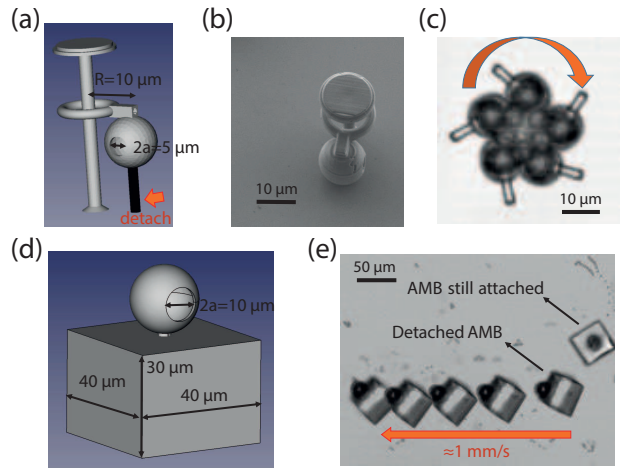

Figure 4: (a) Spinner design; (b) Fabricated spinner (SEM image); (c) AMB spinning at $175 \, \mathrm{Hz}$ under actuation with $P_{ac} = 96.2$ kPa and $f_{transd} = 500$ kHz; (d) AMB and pedestal; (e) Moving AMB with $P_{ac} = 5.6$ kPa.

to detach them. To quantify the propulsion the AMBS generate, we designed a two-part "spinner": a pole and a legged AMB connected to a ring (see Fig. 4a). The probe frees the latter part: it is buoyant but blocked by the top hat. The streaming propels the AMB which rotates around the central pole (Fig. 4c). We achieved a rotation frequency of $f_{rot} = 175 \, \mathrm{Hz}$. If we assume the thrusting force F_{thr} is equal to the Stokes' drag $6\pi\eta r v$, with $v = 2\pi R f_{rot}$ and R gyration radius (see Fig. 4a), then we measure a force of $F_{thr} = 0.75$ nN. This thrust is in good agreement with the analytic thrust prediction of Eq. 2. Note that this is a powerful thrust, two orders of magnitude larger than the buoyancy force acting on a $12 \, \mu m$ bubble.

VII. CONCLUSION

To conclude, in this paper we have fabricated and tested devices in the 10-20 μm range able to generate contactless acoustic propulsion from stabilised microbubbles lasting hours. Our results are promising for future studies on other self-travelling microobjects, as basic elements for controlled active assemblies, and ultimately for applications in mixing and transport. For that purpose, we have also fabricated an AMB mounted on a solid pedestal countering the bubble buoyancy once freed. In Fig. 4e we show a free AMB next to one which is still attached. The free AMB is propelled at speeds of order 1 mm/s solely by the bubble-based steady streaming ($F_{thr} \approx 0.6$ nN). This velocity is on the order of magnitude required to travel in blood capillaries or to be efficiently used for mixing [21]. Future improvements will include designing multiple bubble swimmers and fixed legged AMBs acting as mixing agents in microchannels.

[1] JianFeng and S.K. Cho, Mini and micro propulsion for medical swimmers, Micromachines, **5**, 97–113, (2014).JianFeng; Cho, S.K.

[2] D. Patra, S. Sengupta, W. Duan, H. Zhang, R. Pavlick and A. Sen, Intelligent, self-powered, drug delivery systems, Nanoscale, **5**, 1273–1283 (2013).

[3] B. J. Nelson, I. K. Kaliakatsos and J. J. Abbott, Microrobots for minimally invasive medicine, Annual Review of Biomedical Engineering, **12**, 55–85, (2010).

[4] P. Baldeck, O. Stephan and C. Andraud, BASICS AND APPLICATIONS OF PHOTOPOLYMERIZATION REACTION, ed. J. Fouassier and X. Allonas, (Research Signpost), (2010), vol. 3, ch. Tri-dimentional microstructuration of materials by two-photon induced photochemistry, pp. 199–220.

[5] J. Feng, J. Yuan and S. K. Cho, Micropropulsion by an acoustic bubble for navigating microfluidic spaces, Lab Chip, **15**, 1554–1562, (2015).

[6] R. Dreyfus, J. Baudry, M. L. Roper, M. Fermigier, H. A. Stone and J. Bibette, Microscopic artificial swimmers, Nature (London), **437**, 862–865, (2005).

[7] A. Snezhko, M. Belkin, I. S. Aranson and W.-K. Kwok, Self-Assembled Magnetic Surface Swimmers, Phys. Rev. Lett., **102**, 118103, (2009).

[8] L. Zhang, J. J. Abbott, L. Dong, K. E. Peyer, B. E. Kratochvil, H. Zhang, C. Bergeles and B. J. Nelson, Characterizing the swimming properties of artificial bacterial flagella, Nano Letters, **9**, 3663–3667, (2009).

[9] W. F. Paxton, K. C. Kistler, C. C. Olmeda, A. Sen, S. K. St. Angelo, Y. Cao, T. E. Mallouk, P. E. Lammert and V. H. Crespi, Catalytic nanomotors: autonomous movement of striped nanorods, J. Am. Chem. Soc., **126**, 13424–13431, (2004).

[10] Z. Fattah, G. Loget, V. Lapeyre, P. Garrigue, C. Warakulwit, J. Limtrakul, L. Bouffier and A. Kuhn, Straightforward single-step generation of microswimmers by bipolar electrochemistry, Electrochim. Acta, **56**, 10562–10566, (2011).

[11] R. J. Dijkink, J. P. v. d. Dennen, C. D. Ohl and A. Prosperetti, The 'acoustic scallop': a bubble-powered actuator, J. Micromech. Microeng., **16**, 1653–1659, (2006).

[12] D. Ahmed, X. Mao, J. Shi, B. K. Juluri and T. J. Huang, A millisecond micromixer *via* single-bubble-based acoustic streaming, Lab Chip, **9**, 2738–2741, (2009).

[13] D. Ahmed, M. Lu, A. Nourhani, P. E. Lammert, Z. Stratton, H. S. Muddana, V. H. Crespi, and T. J. Huang, Selectively manipulable acoustic-powered microswimmers, Sci. Rep., **5**, 9744, (2015).

[14] B. Cox, Acoustics of Ultrasound Imaging, Lecture Notes, University College London, (2013).

[15] T. G. Leighton, THE ACOUSTIC BUBBLE, (Academic Press), (London), (1994).

[16] P. Marmottant and S. Hilgenfeldt, Controlled vesicle deformation and lysis by single oscillating bubbles, Nature (London), **453**, 153–156, (2003).

[17] C. Wang, S. V. Jalikop and S. Hilgenfeldt, Size-sensitive sorting of microparticles through control of flow geometry, Appl. Phys. Lett., **99**, 034101, (2011).

[18] P. S. Epstein and M. S. Plesset, On the stability of gas bubbles in liquid-gas solutions, J. Chem. Phys., **18**, 1505–1509, (1950).

[19] C.-Y. Liao, M. Bouriau, P. L. Baldeck, J.-C. Leon, C. Masclet and T.-T. Chung, A two dimensional slicing method to speed up the fabrication of micro-objects based on two-photon polymerization, Applied Physics Letters, **91**, 033108, (2007).

[20] C. Wang, B. Rallabandi and S. Hilgenfeldt, Frequency dependence and frequency control of microbubble streaming flows, Phys. Fluids, **25**, 022002, (2013).

[21] E. N. Marieb and K. Hoehn, Human anatomy and physiology, 9th ed., Pearson Education Inc., ch. The cardiovascular system: blood vessels, p. 712, (2013).

[22] N. T. Ouellette, H. Xu and E. Bodenschatz, A quantitative study of three-dimensional Lagrangian particle tracking algorithms, Exp. Fluids, **40**, 301–313, (2006).

[23] T. A. Spelman and E. Lauga, Arbitrary axisymmetric steady streaming: Flow, force and propulsion, arXiv:1512.00048 [physics.flu-dyn], (2015).

[24] C. Eckart, Vortices and streams caused by sound waves, Phys. Rev., **73**, 68–76, (1948).

[25] N. Riley, Steady streaming, Annu. Rev. Fluid Mech., **33**, 43–65, (2001).

[26] W. L. Nyborg, Acoustic streaming near a boundary, J. Acoust. Soc. Am., **30**, 329–339, (1958).

[27] S. A. Elder, Cavitation microstreaming, J. Acoust. Soc. Am., **31**, 54–64, (1958).

[28] N. Riley, On a sphere oscillating in a viscous liquid, Q. J. Mech. Appl. Math., **19**, 461–472, (1966).

[29] B. J. Davidson and N. Riley, Cavitation microstreaming, J. Sound Vib., **15**, 217–233, (1971).

[30] M. S. Longuet-Higgins, Viscous streaming from an oscillating spherical bubble, P. Roy. Soc. Lond. A Mat, **454**, 725–742, (1998).

[31] A. O. Maksimov, Viscous streaming from surface waves on the wall of acoustically-driven gas bubbles, Eur. J. Mech. B-Fluid, **26**, 28–42, (2007).

[32] H. Ishida and Y. Shigenaka, Cell model contraction in the ciliate spirostomum, Cell Motil. Cytoskel., **9**, 278–282, (1988).

[33] J. R. Blake, A note on the image system for a stokeslet in a no slip boundary, Proc. Camb. Phil. Soc., **70**, 303–310, (1971).

[34] J. R. Blake and A. T. Chwang, Fundamental singularities of viscous flow. Part I. The image systems in the vicinity of a stationary no-slip boundary, J. Eng. Math, **8**, 23–29, (1974).